

Interactive model of Purcell-Dicke enhancement

Richard Friedberg

Department of Physics, Columbia University, New York, New York 10027, USA

Jamal T. Manassah*

Department of Electrical Engineering, City College of New York, New York, New York 10031, USA

(Received 20 April 2012; published 3 August 2012)

We compute the design parameters that maximize the cooperative decay rate (CDR) from a nanosphere of identical two-level atoms phased to radiate coherently (Dicke enhancement), encased in a shell of a noble metal (Purcell effect), the whole suspended for mechanical support in a dielectric medium extending to infinity. Both the radiating core and the metallic shell are described internally by their respective frequency-dependent dielectric functions. (In previous papers one or the other medium was given a fixed dielectric constant.) The solution is noticeably altered, and the enhancement increased, when both media respond interactively to one another.

DOI: [10.1103/PhysRevA.86.023804](https://doi.org/10.1103/PhysRevA.86.023804)

PACS number(s): 42.50.Nn, 42.50.Pq

I. INTRODUCTION

In 1946, Purcell [1] pointed out that the spontaneous rate of an atom should be enhanced if the atom were coupled to a macroscopic resonant circuit of high quality and small volume. In 1954, Dicke [2] introduced the idea of superradiance, in which a large number N of atoms radiate coherently when suitably phased, like an array of tuning forks or the parts of an antenna. The two phenomena have been extensively discussed [3] over the intervening decades, but as separate fields of physics; even when an extended radiating source is studied for the Purcell effect, the atoms are supposed to radiate independently so that the Dicke effect is not included. In this paper we study a system in which the two effects are combined.

Both the Purcell and the Dicke effect have been studied in many geometries. To obtain a clean calculation, we choose a particular scenario with spherical symmetry: the active atoms are distributed uniformly in a spherical core surrounded by a spherical shell of metallic composition. This makes it possible to treat both regions with a similar formalism. The cooperative effect described by Dicke is captured by giving the core region an electric permittivity depending on the frequency, with a pole at the isolated atom frequency. The behavior of the metal is described by using the Drude formula [4] for the permittivity.

We then seek an interactive eigenmode in which the fields in both regions share a common eigenfrequency, from which the index of refraction of each material is computed as the square root of its permittivity. By eliminating the frequency, we obtain a relation between the wave numbers of the two regions. A second relation is obtained by coupling the two regions through boundary conditions at their common interface. In this way the eigenfrequency is determined to be one of the discrete solutions of a transcendental equation. The complete description of the eigenmode is then obtained in terms of spherical Bessel functions.

In such treatments of the Dicke problem, the eigenfrequency comes out with a negative imaginary part, representing the decay rate. This results in a negative imaginary part for the wave number, so that the magnitude of the field grows as one travels in the direction of wave propagation. Thus the Dicke cooperative effect is represented by the active core being an amplifying, not an absorptive, medium. This is actually a more accurate description of coherent radiation, for general geometries, than the one given in Ref. [2].

We are interested here in optical transitions in the radiating atoms. To achieve the Purcell condition of one (or a few) macroscopic mode(s), we take the radius of the sphere to be smaller than the wavelength of the atomic transition. It has been shown in a different context [5] that with two boundary interfaces (inner and outer radius of the shell) there are just two modes that have a wavelength greater than or equal to that of the resonant light. All other modes have shorter wavelengths and are weakly coupled to the radiation.

At the same time we let the medium outside the shell, which is needed for mechanical support and has its own (fixed) dielectric constant, stretch out very far, so that we may take its radius to be infinite in our equations. Thus outgoing boundary conditions are imposed at the outer radius of the shell.

In two previous papers, this problem was explored by giving one of the two regions a fixed permittivity (dielectric constant) and treating the other by its proper intrinsic equation. In Ref. [6], the pole formula was used for the radiating core but the complex permittivity of the metal was held fixed. The main finding of the paper was that it is possible to adjust the resistivity of the metal so that, on the one hand, the Q value of the cavity is high enough to produce large Purcell enhancement, but on the other hand, the Q value is low enough so that the radiation is not trapped inside the sphere. It was noted in Ref. [6], however, that no account was taken of the dependence of the metallic permittivity on the frequency.

In Ref. [7], the Drude formula was used for the metal but the core was given a fixed real dielectric constant. This treatment simply explored the two long-wavelength modes of a metallic cavity with a passive core, as a function of geometry (thickness

*jmanassah@gmail.com

of shell). It was found that the higher-frequency branch has a frequency whose real part is nearly independent of geometry, while the lower-frequency branch has a frequency that covers a wide range as the geometry is altered. Thus the attainable frequencies fall into two bands, a narrow upper band and a wide lower band.

In the present paper, there is competition between the metallic region, described by the Drude model, and the active region, described by its pole formula, to determine the actual frequency of the mode. For the range of numerical values used here, the metallic constraint is stronger so that the actual frequency falls approximately into either of the two bands found in Ref. [7]. Thus the Purcell effect is weak or absent unless the resonance frequency of the active atoms falls into one of these plasmonic bands, and the geometry is also tuned so as to bring the actual frequency close to the resonance frequency.

When this tuning is achieved, the mode corresponding to the selected branch develops a decay rate, represented by the imaginary part of the actual eigenfrequency, considerably larger than the Dicke prediction for cooperative radiation. By substituting this complex value of frequency into the Drude formula, one finds a permittivity whose imaginary part is less than that found at the (real) resonance frequency. This change further enhances the decay rate, which again feeds into the Drude formula. In our calculation, these mutual effects of the two regions (active core and metallic coating) on one another are taken into account simultaneously rather than iteratively, so that we obtain a Purcell enhancement that can substantially exceed that obtained by simply combining the results of Refs. [6] and [7].

For a very small sphere with no resistive losses, the boundary value problem may be solved electrostatically [8]. The present paper improves on that treatment (a) by including resistive losses through the Drude formula; (b) by including radiative losses [9] through the outgoing boundary conditions; and (c) by including the finite size effects and radiation reaction effects through the use of Bessel functions in the field equation solution.

The results of this paper are the following: (a) a sizable enhancement in the cooperative decay rate (CDR, or shortening in the superradiant lifetime) is observed because of the presence of the metallic shell, (b) the CDR enhancement is maximized when the value of the atomic transition frequency falls within the allowed bands of the eigenfrequencies of the metallic shell, (c) the maximum enhancement is noticeably greater than if the permittivity of the metal were not allowed to be affected by the amplifying nature of the radiative core, and (d) the maximum enhancement is actually reached within a narrow range in the value of the ratio of the inner to outer radius of the metallic shell.

The paper is organized as follows: In Sec. II, we define our notation in this paper and relate it to notations in our previous works. In Sec. III, we review the constitutive equations in each region of space. In Sec. IV, we give the form of the eigenmodes in spherical configuration, the boundary conditions, and the secular determinant relating the wave numbers of the different regions. In Sec. V, we summarize the results that we obtain for different values of the parameters. We conclude in Sec. VI.

II. NOTATION

We use Gaussian units throughout. We designate the three regions by the letters A , B , and C from the outside in, thus

$$A \text{ (passive dielectric)} : r \geq R, \quad (1)$$

$$B \text{ (metal)} : \beta R \leq r \leq R, \quad (2)$$

$$C \text{ (active core)} : r \leq \beta R, \quad (3)$$

where $0 \leq \beta \leq 1$. Thus R is the outer radius of the shell, and βR is the inner radius. (This follows the usage of Ref. [7], but in Ref. [6] R is the inner radius, and the outer radius is αR with $\alpha \geq 1$.)

The eigenmodes of Maxwell's equations in spherical geometry [10–12] are designated by angular indices l and m (corresponding to the spherical harmonics Y_l^m) and a radial index s as well as a binary choice (E or M), where E and M refer, respectively, to the electric and magnetic modes. We limit our attention to the cylindrically symmetric electric dipole modes, $E_{l,m,s} = E_{1,0,s}$. Accordingly we suppress the subscripts $l = 1$ and $m = 0$ and keep only the subscript s . Hence the common (complex) eigenfrequency for a decay mode is called ω_s and the associated wave numbers are k_s^A , k_s^B , and k_s^C . The resonant frequency of the active atoms in the core (when isolated) is ω_0 , and the corresponding wave number in the vacuum is $k_0 = \omega_0/c$.

III. CONSTITUTIVE EQUATION IN EACH REGION

In each region there is a constitutive equation, specific to the material occupying that region, that links the wave number in that material to the complex eigenfrequency.

In region A , (the passive dielectric) we have simply

$$(k_s^A)^2 = \varepsilon^A \omega_s^2 / c^2, \quad (4)$$

where ε^A is a fixed (real) number, independent of the mode.

In region B (the metal shell) we have

$$(k_s^B)^2 = \varepsilon_s^B \omega_s^2 / c^2, \quad (5)$$

where ε_s^B is given by the Drude formula,

$$\varepsilon_s^B(\omega_s) = \varepsilon_\infty^B - \frac{\omega_p^2}{\omega_s^2 + i\gamma\omega_s}, \quad (6)$$

where ω_p is the bulk plasma frequency of the metal, determined from the density of free electrons in the metal and the effective mass of the electron, γ is the electron collision frequency in the bulk metal, and ε_∞ is a phenomenological parameter called the high-frequency part.

We follow some authors in calling ε_s^B a permittivity rather than a dielectric function, in that the equation $\vec{D} = \varepsilon_s^B \vec{E}$ requires a physical picture in which the conduction current is regarded as a movement of bound charge with no restoring force. In this picture the term $4\pi \vec{J}$ in Maxwell's equations is included in \vec{D} so that \vec{J} no longer appears explicitly; instead the divergence of \vec{D} is now zero (rather than $4\pi\rho$), and the curl of \vec{H} is simply $\dot{\vec{D}}$, rather than $4\pi \vec{J} + \dot{\vec{D}}$.

In our illustrations in Sec. V, we adopt, for the optical regime, Sonnichsen's values for gold [13], namely,

$$\text{Au} : \varepsilon_\infty = 9.8, \lambda_p = 136 \text{ nm}, \text{ and} \\ \Gamma = \gamma/\omega_p = 6.94 \times 10^{-3}.$$

In region C (the active atoms) we have

$$(k_s^C)^2 = \varepsilon_s^C(\omega_s) \omega_s^2/c^2, \quad (7)$$

where $\varepsilon_s^C(\omega_s)$ is given by the resonance pole formula,

$$\varepsilon_s^C(\omega_s) = 1 - \frac{C}{\omega_s - \omega_0 + \omega_L + i\gamma_T}. \quad (8)$$

Here $C = 4\pi\wp^2 n/\hbar$, n is the atomic number density, \wp is the reduced dipole matrix element for the two-level transition, $\omega_L = \frac{1}{3}C$ is the Lorentz shift due to the Clausius-Mossotti local field correction, and γ_T is the collisional half-width of the line ($\gamma_T \cong 0.6C$) [14].

It is to be noted that the Kramers-Kronig relation, which requires only causality for its validity, allows the susceptibility and consequently the dielectric function to be analytically continued in the lower half of the complex-frequency plane. This allows us to use the same functional form of ε^C for complex ω_s as the familiar one for real ω . Since $\text{Im}(\omega_s)$ is negative for a decaying system, it is possible for $\text{Im}(\omega_s + i\gamma_T)$ to be negative, so that Eq. (8) may represent an amplifying medium, although it would be absorbing if ω_s were real.

IV. EIGENMODES IN SPHERICAL CONFIGURATION

A. Fields and boundary conditions

For a cylindrically symmetric dipole mode $E_{1,0,s}$, the expressions for \vec{B} and \vec{E} in any one of the three regions depend on two constant coefficients specific to that region, but otherwise have the same form in each region. Letting F_i stand for A_i , B_i , or C_i in each respective region, where $i = 1$ or 2 , we have

$$\vec{B}(r, \theta, \varphi) = [F_1 j_1(k_s^F r) + F_2 n_1(k_s^F r)] P_1^1[\cos(\theta)] \hat{e}_\varphi \quad (9)$$

and

$$\vec{E}(r, \theta, \varphi) = -\frac{i k_0}{(k_s^F)^2 r} (2 [F_1 j_1(k_s^F r) + F_2 n_1(k_s^F r)] P_1[\cos(\theta)] \hat{e}_r \\ + \{F_1 [(k_s^F r) j_0(k_s^F r) - j_1(k_s^F r)] + F_2 [(k_s^F r) n_0(k_s^F r) - n_1(k_s^F r)]\} P_1^1[\cos(\theta)] \hat{e}_\theta), \quad (10)$$

where $P_1[\cos(\theta)] = \cos(\theta)$ and $P_1^1[\cos(\theta)] = -\sin(\theta)$ are the Legendre polynomial and the associated Legendre function, and j_0, j_1 and n_0, n_1 are, respectively, zeroth- and first-order spherical Bessel and Neumann functions.

To avoid a singularity at $r = 0$, we must have

$$C_2 = 0, \quad (11)$$

and to have a pure outgoing wave in $r > R$, we must have

$$A_2 = i A_1. \quad (12)$$

In addition, Maxwell's equations require continuity of B_φ and E_θ at the boundaries $r = \beta R$ and $r = R$:

$$C_1 j_1(k_s^C \beta R) = B_1 j_1(k_s^B \beta R) + B_2 n_1(k_s^B \beta R), \quad (13)$$

$$(k_s^C \beta R)^{-2} C_1 [k_s^C \beta R j_0(k_s^C \beta R) - j_1(k_s^C \beta R)] \\ = (k_s^B \beta R)^{-2} \{B_1 [k_s^B \beta R j_0(k_s^B \beta R) - j_1(k_s^B \beta R)] \\ + B_2 [k_s^B \beta R n_0(k_s^B \beta R) - n_1(k_s^B \beta R)]\}, \quad (14)$$

and

$$B_1 j_1(k_s^B R) + B_2 n_1(k_s^B R) = A_1 h_1^{(1)}(k_s^A R), \quad (15)$$

$$(k_s^B R)^{-2} \{B_1 [k_s^B R j_0(k_s^B R) - j_1(k_s^B R)] + B_2 [k_s^B R n_0(k_s^B R) - n_1(k_s^B R)]\} \\ = (k_s^A R)^{-2} A_1 [k_s^A R h_0^{(1)}(k_s^A R) - h_1^{(1)}(k_s^A R)], \quad (16)$$

where $h_l^{(1)}(u) = j_l(u) + i n_l(u)$.

It is through Eqs. (13) and (14) that the radiating atoms in C are coupled to the ‘‘resonant circuit’’ provided by the metal in B .

B. Dimensionless notation

Before proceeding further, we replace the wave numbers by dimensionless equivalents:

$$u_0 = k_0 R, \quad (17)$$

$$u_s^A = k_s^A R, \quad (18)$$

$$u_s^B = k_s^B R, \quad (19)$$

$$u_s^C = k_s^C R. \quad (20)$$

In the previous two papers, Refs. [6] and [7], different nomenclatures were used for these dimensionless parameters. In each there was only one ‘‘responsive’’ region—that is, where ε was ω dependent—and for this region the letter ‘‘ u ’’ was replaced by ‘‘ v .’’ Thus v_s was used for region C in Ref. [6] and for region B in Ref. [7]. Also, in Ref. [6] the radius R pertained to the B - C boundary, whereas here and in Ref. [7] it describes the A - B boundary. A comparison of the notation used in these three papers is given in Table I.

C. Secular determinant

Equations (13)–(16) are a set of four linear homogeneous equations in the four unknowns: A_1 , B_1 , B_2 , and C_1 . For a solution to exist, the characteristic secular determinant for

TABLE I. Comparison of notation used here with that in Refs. [6] and [7].

Ref. [6]	Ref. [7]	This paper
R	βR	βR
αR	R	R
α^{-1}	β	β
u_0	βu_0	βu_0
v_s	βu_c	βu_s^C
u	βv_s	βu_s^B
w	βu_m	βu_s^A

this system must vanish; in terms of the dimensionless wave numbers introduced above,

$$\det \begin{pmatrix} j_1(u_s^C \beta) & -j_1(u_s^B \beta) & -n_1(u_s^B \beta) & 0 \\ (u_s^B)^2 j_V(u_s^C \beta) - (u_s^C)^2 j_V(u_s^B \beta) & -(u_s^C)^2 n_V(u_s^B \beta) & 0 & 0 \\ 0 & j_1(u_s^B) & n_1(u_s^B) & -h_1^{(1)}(u_s^A) \\ 0 & (u_s^A)^2 j_V(u_s^B) & (u_s^A)^2 j_V(u_s^B) & -(u_s^B)^2 h_V^{(1)}(u_s^A) \end{pmatrix} = 0, \quad (21)$$

where we have written $j_V(u)$ for $u j_0(u) - j_1(u)$, and likewise $n_V(u)$ and $h_V^{(1)}(u)$.

We observe that the constitutive equations from Sec. II have played no part in the reasoning leading to Eq. (21). Hence this reasoning, apart from notation, is identical to that given in Refs. [6,7]. The reader may verify (using Table I) the complete correspondence between Eq. (21) and the $(4 \otimes 4)$ matrices given in each of those papers. Equation (21), however, is not sufficient to determine the eigenfrequencies and wave numbers because it contains three unknowns: $u_s^A = k_s^A R$, $u_s^B = k_s^B R$, and $u_s^C = k_s^C R$. It is now necessary to obtain two more equations between these quantities. We shall use the constitutive equations [Eqs. (4)–(8)] to obtain the additional two equations required to solve for the three wave numbers. From Eq. (4) we obtain

$$(u_s^A)^2 = \varepsilon^A u_0^2, \quad (22)$$

which determines u_s^A independently of ω_s .

We then solve Eqs. (7) and (8) for ω_s , obtaining

$$\omega_s = \omega_0 - i \Lambda C, \quad (23a)$$

where

$$-i \Lambda = \left(\frac{u_0^2}{u_0^2 - (u_s^C)^2} - \frac{\omega_L}{C} - i \frac{\gamma_T}{C} \right). \quad (23b)$$

Then we substitute Eq. (23a) into Eqs. (5) and (6) to get

$$\frac{(u_s^B)^2}{u_0^2} = \varepsilon_\infty - \frac{1}{(\Omega - i \Lambda \chi)^2 + i \Gamma (\Omega - i \Lambda \chi)}, \quad (23c)$$

with the dimensionless parameters $\Gamma = \frac{\gamma}{\omega_p}$, $\Omega = \frac{\omega_0}{\omega_p}$, and $\chi = \frac{C}{\omega_p}$.

Equations (23c) and (23b) give us the relation between u_s^B and u_s^C , this and Eq. (22) are the additional equations required to supplement Eq. (21). This gives a transcendental equation in u_s^C which we solve numerically. In our numerical search for roots we select the two roots with $\text{Re}(u_s^C) > 0$ closest to 0 and $\text{Im}(u_s^C) < 0$.

Having computed $u_s^A = k_s^A R$, $u_s^B = k_s^B R$, and $u_s^C = k_s^C R$ as functions of u_0 and the physical parameters, the quantities B_1/C_1 , B_2/C_1 , and A_1/C_1 are uniquely determined by

solving

$$\begin{pmatrix} j_1(u_s^B \beta) & n_1(u_s^B \beta) & 0 \\ j_1(u_s^B) & n_1(u_s^B) & -h_1^{(1)}(u_s^A) \\ (u_s^A)^2 j_V(u_s^B) & (u_s^A)^2 n_V(u_s^B) & -(u_s^B)^2 h_V^{(1)}(u_s^A) \end{pmatrix} \begin{pmatrix} B_1/C_1 \\ B_2/C_1 \\ A_1/C_1 \end{pmatrix} = \begin{pmatrix} j_1(u_s^C \beta) \\ 0 \\ 0 \end{pmatrix}. \quad (24)$$

V. RESULTS

As preparation we show in Figs. 1 and 2 some results from Ref. [7]. In Fig. 1 we plot the real and imaginary parts of the index of refraction of the metal, as given by the present Eq. (6) with ω_s replaced by a real variable ω . Because of the large value of ε_∞ in gold, the ‘‘plasma transition’’ from near opacity (low ω) to transparency (high ω) takes place not at the plasma frequency ω_p , but at about one-third that frequency.

Figure 2 shows the actual frequencies of the two modes of the empty shell, as functions of geometry as represented by the parameter β . The upper frequency lies in a narrow band located in the opaque region of Fig. 1, close to the plasma transition. The lower frequency, sensitive to β , lies in a wide band reaching down essentially to zero. These are the ‘‘plasmonic bands.’’

Figures 3 and 4 exhibit results of the calculations from Eqs. (21)–(24) in the present paper. Our main concern here is the decay rate $\text{Im}(\omega_s) = C \text{Re}(\Lambda)$ (see Eq. (23a)). But not all of this decay rate represents coherent radiation from the active region. Some of it is loss of coherence due to collision broadening within that region, measured by the rate γ_T . The true superradiant rate is really $\text{Im}(\omega_s) - \gamma_T = C \text{Re}(\tilde{\Lambda})$, where

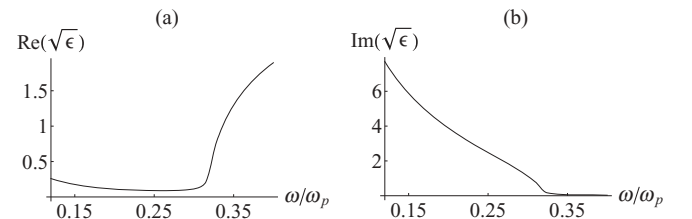


FIG. 1. The (a) real and (b) imaginary parts of the index of refraction of gold are plotted as functions of the ratio of the light frequency to the plasma frequency using Sonnichsen’s values for the parameters of the Drude model.

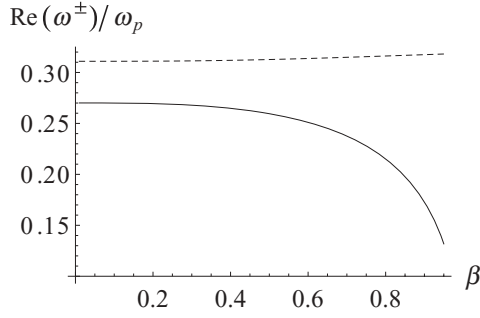


FIG. 2. The ratios of the plasmonic resonance frequency to the plasma frequency in gold are plotted as functions of β (+ is the upper trace, and - is the lower trace). $u_0 = 0.2$, $n_m = 4/3$, and $n_c = 1$ (empty core).

$\tilde{\Lambda} = \Lambda - \gamma_T/C$. Therefore in Figs. 3 and 4 it is $\text{Re}(\tilde{\Lambda})$ that we plot.

The enhancement factor

$$\eta = \frac{\text{Re}(\tilde{\Lambda})}{\Lambda_D} \quad (25)$$

is obtained by dividing $C\text{Re}(\tilde{\Lambda})$ by the Dicke superradiant rate which corresponds to the superradiant rate at $\beta = 1$ (no metallic shell). The Dicke rate for a small sphere is [10]

$$C\Lambda_D = \frac{2Cn_m^5}{(1 + 2n_m^2)^2} u_0^3. \quad (26)$$

In Figs. 3(a)–3(d) we plot $\text{Re}(\tilde{\Lambda})$ against β , for four different values of the atomic resonance frequency ω_0 : (a) well above the upper plasmonic band, (b) within the upper band, (c) between the two bands, and (d) well into the lower band. In all cases $u_0 = 0.2$ and $n_m = 4/3$, giving $\Lambda_D = 0.00325$ from Eq. (26).

We see that in Figs. 3(b) and 3(d) there is Purcell enhancement [$\text{Re}(\tilde{\Lambda})/\Lambda_D$] exceeding 2 orders of magnitude at the “best” value of β , whereas in Fig. 3(c) there is only

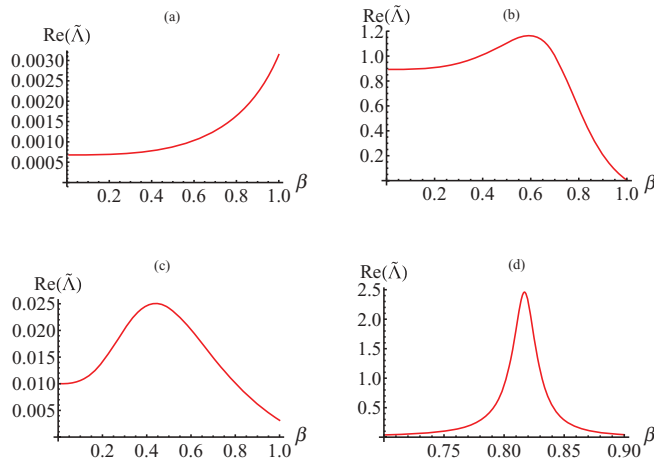


FIG. 3. (Color online) The normalized CDR of the atomic ensemble is plotted as a function of β for different values of the ratio of the atomic transition frequency to the metal plasma frequency. $u_0 = 0.2$, $n_m = 4/3$, and $\chi = 10^{-4}$. (a) $\omega_0/\omega_p = 0.5$. (b) $\omega_0/\omega_p = 0.315$. (c) $\omega_0/\omega_p = 0.28$. (d) $\omega_0/\omega_p = 0.21$.

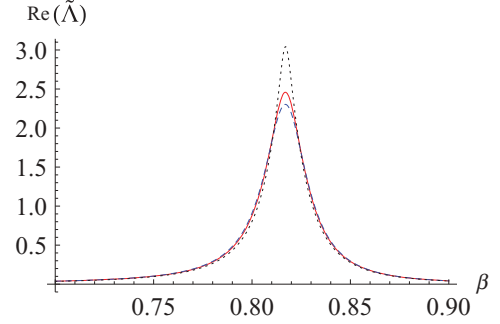


FIG. 4. (Color online) The normalized CDR of the atomic ensemble is plotted as a function of β for different values of $\chi = C/\omega_p$. $u_0 = 0.2$, $n_m = 4/3$, $\omega_0/\omega_p = 0.21$. Dashed line: $\chi = 10^{-5}$. Solid line: $\chi = 10^{-4}$. Dotted line: $\chi = 3 \times 10^{-4}$.

an eightfold enhancement and in Fig. 3(a) there is none at all because ω_0 is far from the bands. In Fig. 3(b) there is strong enhancement for all $\beta < 0$ because of the flatness of the upper plasmonic band in Fig. 2. In Fig. 3(d), the large geometry dependence of the lower band causes the enhancement to fade away rapidly [note the scale of the abscissa in Fig. 3(d)] as one departs from the peak at $\beta = 0.816$. The maximum enhancement η is 782, compared to 370 in Fig. 3(b).

These figures exhibit the necessity for the atomic resonance frequency to lie within a plasmonic band of the metal, in order to obtain large Purcell enhancement. In the analysis of Ref. [6], there was no comparable band structure because the frequency of the cavity resonance had only a smooth variation with geometry. (The large enhancement of ~ 5000 obtained in Ref. [6] was possible because the metallic permittivity could be set arbitrarily, whereas in the present paper it is tied to the characteristics of a real metal, gold.)

In Fig. 4 we study the effect noted in the Introduction of the mutual influence between the two regions B and C leading to an increase in the Purcell enhancement. We call this effect “ B - C coupling.” Let us first observe that Eq. (23b) gives us

$$-i\tilde{\Lambda} = -i\left(\Lambda - \frac{\gamma_T}{C}\right) = \frac{u_0^2}{u_0^2 - (u_s^C)^2} - \frac{1}{3}, \quad (27)$$

since C is defined to be $3\omega_L$. Thus $\tilde{\Lambda}$ is related to u_s^C in a way independent of C . However, u_s^C is itself determined by eliminating Λ between Eqs. (23b) and (23c), expressing u_s^B in terms of u_s^C and u_s^A by Eq. (22), and solving Eq. (21). In

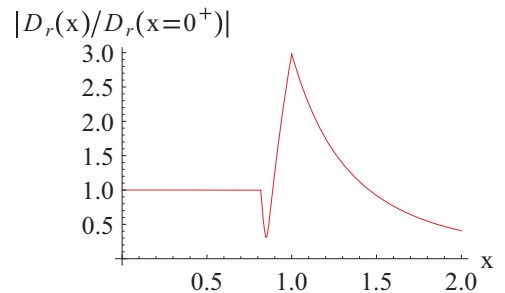


FIG. 5. (Color online) The radial component of the displacement vector is plotted as a function of the normalized radius, at the maximum decay rate of Fig. 3(d).

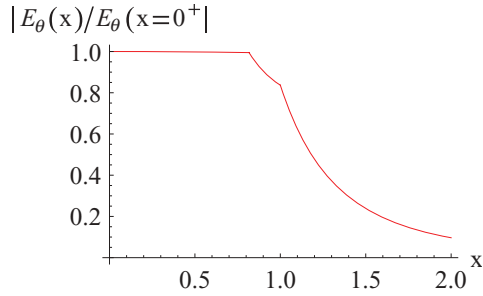


FIG. 6. (Color online) The tangential component of the electric field is plotted as a function of the normalized radius, at the maximum decay rate of Fig. 3(d).

this process the value of C enters through the appearance of $\chi = C/\omega_p$ in Eq. (23c).

Thus we study the effect of C on $\text{Re}(\tilde{\Lambda})$ by displaying in Fig. 4 the result of varying χ in the calculation leading to Fig. 3(d). We obtain three curves, which are essentially identical except in the region of the peak. The middle curve in Fig. 4 corresponds to Fig. 3(d); the uppermost curve has χ three times greater; and the lowermost has χ so small that it might as well be zero. The peak of the curve is the portion where $-\text{Im}(\omega_s) = C\text{Re}(\Lambda) = C\text{Re}(\tilde{\Lambda}) + \gamma_T$ is greatest. Therefore the difference among the three curves must reflect the effect of using the complex frequency ω_s in Eq. (6), rather than its real part ω . Indeed, the expression $\Omega - i\chi\Lambda$ appearing in Eq. (23c) is just ω_s/ω_p according to Eq. (23a).

In this way the activity of the atoms in the core, represented by the value of χ , is able to affect the permittivity of the metal in region B . In fact, since at the maximum Ω , Λ , χ , and Γ are all real, the imaginary part of the denominator in Eq. (23c) is just $\Omega(\Gamma - 2\Lambda\chi) = \frac{\omega_0[\gamma + 2\text{Im}(\omega_s)]}{\omega_p^2}$. Thus the migration of the eigenfrequency off the real axis in the negative imaginary direction has precisely the effect of diminishing the “effective” electron collision frequency of the metal, raising the Q value of the cavity and so increasing the enhancement factor η .

If we set $\chi = 0$ in Eq. (23c) and carry out the whole calculation otherwise as before, we obtain the result of neglecting the B - C coupling. This is closely approximated by the lowest curve in Fig. 4. The peak value of $\text{Re}(\tilde{\Lambda})$ is then 2.30, whereas in the highest curve it is 3.04. Thus the B - C coupling arising from a value of C equal to $3 \times 10^{-4}\omega_p$ is sufficient to produce a 32% increase in the Purcell enhancement factor.

Finally, in Figs. 5 and 6, to test the consistency of our computations, we plot, respectively, the values of D_r and of E_θ for the case considered in Fig. 3(d), and we show that the results obtained are continuous as they should be. Examining Fig 6, we also note that, despite the presence of the metal, the strength of the tangential component of the electric field as it escapes from the metal into the passive dielectric medium has changed only by 20% from its value entering the metal (almost the geometrical factor). This result puts to rest the possible concern that the metal shell may in this instance trap the atomic radiation and prevent it from escaping into the passive medium.

VI. CONCLUSION

In conclusion, by using the interacting model for both the atomic medium and the electron in the metals, i.e., using the frequency-dependent dielectric functions for both materials, we clarified the physical picture describing the cause for the enhancement of the superradiance rate for a sphere of identical atoms enclosed in a thin shell of gold and obtained accurate values for this quantity at its maximum in each configuration.

The eigenmode approach employed here gives directly the time evolution of superradiance following excitation by a short pulse. In principle, the same information could be acquired by a somewhat roundabout method based on Mie scattering [15]. In the scattering method, one would decompose the short pulse setting up the initial excitation by a Fourier analysis in time and solve the boundary value problem for general real frequency. To get the time development of the system, one must multiply each frequency component by its time factor $\exp(-i\omega t)$ and then integrate over ω . In many situations this may be easier than summing over the discrete complex frequencies corresponding to free decay. But here only two complex frequencies need to be included, so that the eigenmode treatment is easier and more accurate.

By stretching a point, one may regard the Dicke cooperative enhancement of CDR as a special kind of Purcell enhancement in which, for each radiating atom, the ensemble of all the other active atoms acts as the macroscopic resonant circuit. We have, however, chosen not to press this analogy here.

ACKNOWLEDGMENTS

We are grateful to Prashant Jain for helpful communications.

- [1] E. M. Purcell, *Phys. Rev.* **69**, 681 (1946).
- [2] R. H. Dicke, *Phys. Rev.* **93**, 99 (1954).
- [3] M. Gross and S. Haroche, *Phys. Rep.* **93**, 301 (1982); J. M. Gerard, *Topics Appl. Phys.* **90**, 269 (2003).
- [4] M. M. Alvarez, J. T. Khoury, G. Shaaff, M. N. Shafiqulin, I. Vezmar, and R. L. Whetten, *J. Phys. Chem. B* **101**, 3706 (1997).
- [5] R. Friedberg and J. T. Manassah, *Phys. Rev. A* **85**, 013834 (2012).
- [6] J. T. Manassah, *Laser Phys.* **22**, 738 (2012).
- [7] R. Friedberg and J. T. Manassah, *Chem. Phys. Lett.* **539–540**, 118 (2012).
- [8] P. K. Jain and M. A. Al-Sayed, *Chem. Phys. Lett.* **487**, 153 (2010).
- [9] K. L. Kelly, E. Coronado, L. L. Zhao, and G. C. Schatz, *J. Phys. Chem.* **107**, 668 (2003).
- [10] R. Friedberg and J. T. Manassah, *Phys. Lett. A* **372**, 6833 (2008).
- [11] R. Friedberg and J. T. Manassah, *Phys. Lett. A* **373**, 4416 (2009).
- [12] S. Prasad and R. J. Glauber, *Phys. Rev. A* **82**, 063805 (2010).
- [13] C. Sonnichsen, http://edoc.ub.unimuenchen.de/2367/Sonnichsen_Carsten.pdf.
- [14] R. Friedberg, S. R. Hartmann, and J. T. Manassah, *Phys. Rep.* **7**, 101 (1973).
- [15] G. Mie, *Ann. Phys.* **25**, 377 (1908).